Ecological Informatics 79 (2024) 102441

Contents lists available at ScienceDirect

Ecological Informatics

journal homepage: www.elsevier.com/locate/ecolinf

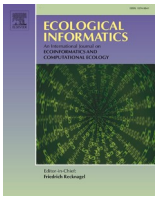

Near-infrared digital hemispherical photography enables correction of plant area index for woody material during leaf-on conditions

Luke A. Brown [a,b,*], Harry Morris [c,b], Rosalinda Morrone [d,c], Morven Sinclair [c], Owen Williams [b], Merryn Hunt [e,b], Subhajit Bandopadhyay [b], Xuerui Guo [f,b], Haydar Akcay [g,b], Jadunandan Dash [b]

[a] School of Science, Engineering & Environment, University of Salford, Manchester M5 4WT, United Kingdom
[b] School of Geography and Environmental Science, University of Southampton, Highfield, Southampton SO17 1BJ, United Kingdom
[c] Climate and Earth Observation Group, National Physical Laboratory, Teddington TW11 0LW, United Kingdom
[d] Downforce Technologies, Botley, Oxford OX2 0JB, United Kingdom
[e] UK Centre for Ecology and Hydrology, Lancaster Environment Centre, Bailrigg, Lancaster LA1 4AP, United Kingdom
[f] Institute of Bio- and Geosciences: Agrosphere (IBG-3), Forschungszentrum Jülich GmbH, 52428 Jülich, Germany
[g] Department of Geomatics Engineering, Civil Engineering Faculty, Istanbul Technical University, 34469 Istanbul, Türkiye

ARTICLE INFO

Keywords:
DHP
Leaf area index (LAI)
Near-infrared imagery
PAI
Wood area index (WAI)

ABSTRACT

Indirect optical measurement techniques enable efficient and non-destructive estimation of plant area index (PAI). However, because they cannot distinguish between foliage and other canopy elements, corrections are needed to determine leaf area index (LAI), which is typically the property of interest. In this study, we investigate near-infrared digital hemispherical photography (DHP) as a means of estimating and correcting for woody material. Using data collected at a deciduous broadleaf forest site, we show that near-infrared DHP could successfully estimate effective wood area index (WAI_e) and wood area index (WAI) during leaf-on conditions, providing similar mean values ($WAI_e = 0.88$, $WAI = 1.53$) to those determined from visible DHP during leaf-off conditions ($WAI_e = 0.87$, $WAI = 1.38$). This information was used to correct estimates of effective PAI (PAI_e) and PAI, enabling effective LAI (LAI_e) and LAI to be derived with low RMSD (0.33 for LAI_e and 0.76 for LAI), NRMSD (12% for LAI_e and 19% for LAI), and bias (−0.01 for LAI_e and −0.16 for LAI). Not correcting for woody material led to overestimation of LAI_e by 31% on average and 46% in the worst observed case, and the degree of overestimation was further enlarged for LAI (42% on average and 61% in the worst observed case). In agreement with previous studies, the effects of clumping and woody area were found to be partly compensatory. On average, PAI_e provided a reasonable approximation of LAI without correction, though overestimation of 52% and underestimation of 20% occurred at the lowest and highest LAI values, respectively. Compared to WAI_e and WAI measurement using leaf-off visible DHP, near-infrared DHP offers two crucial advantages: i) data collection can be conducted at the same time as leaf-on PAI_e and PAI measurements, and ii) it is likely that the approach could provide an indirect WAI_e and WAI measurement option for evergreen species.

1. Introduction

Defined as half the total intercepting area of leaves per unit horizontal ground surface area (Chen and Black, 1991), leaf area index (LAI) is a crucial parameter in defining the vegetated environment, determining size of the interface between the biosphere and atmosphere, and thus the interception of light, which in turn regulates photosynthesis. A related quantity is plant area index (PAI), which incorporates all plant material rather than only leaves, and is represented by the sum of LAI and wood area index (WAI). Of these terms, it is accurate estimates of LAI in particular that are required in a wide range of applications (including modelling vegetation productivity, carbon exchange, and the weather and climate systems), and LAI is designated an essential climate variable (ECV) for this reason (GCOS, 2019; Richardson et al., 2013; Sellers et al., 1997). Direct LAI measurement approaches involve harvesting all leaves from a given portion of ground and measuring their area (Bréda, 2003; Jonckheere et al., 2004). Alternatively, leaves can be weighed, from which LAI can be calculated if leaf mass per area (LMA) or specific leaf area (SLA), which corresponds to the inverse of LMA, is known or has been determined for a smaller subset of leaves (Bréda,

* Corresponding author at: School of Science, Engineering & Environment, University of Salford, Manchester M5 4WT, United Kingdom.
E-mail address: l.a.brown4@salford.ac.uk (L.A. Brown).

https://doi.org/10.1016/j.ecoinf.2023.102441
Received 6 July 2023; Received in revised form 15 December 2023; Accepted 17 December 2023
Available online 22 December 2023

2003; Jonckheere et al., 2004).

The laborious and time-consuming nature of direct LAI measurement approaches led to the development of indirect optical in situ measurement techniques, including ceptometry, digital hemispherical photography (DHP), digital cover photography (DCP), and dedicated instruments such as the LI−COR LAI−2000, LAI—2200C, and Tracing Radiation Architecture of Canopies (TRAC) series of devices (Bréda, 2003; Chen and Cihlar, 1995; Jonckheere et al., 2004; Welles and Norman, 1991; Yan et al., 2019). These techniques enable efficient and non-destructive estimation of effective PAI (PAI_e), in which a random distribution of plant material is assumed, with some also correcting for clumping to enable PAI to be derived. However, because they cannot distinguish between foliage and other canopy elements, corrections are needed to determine LAI, which is typically the property of interest. Because it is easily obtained, in many studies, PAI is simply assumed equal to LAI (Camacho et al., 2013; De Kauwe et al., 2011; Heiskanen et al., 2012; Verger et al., 2011). This may be a reasonable assumption in the case of leafy vegetation types such as grasses, but will lead to considerable biases in the case of forests, where up to 35% of the total plant area may be comprised of woody material (Gower et al., 1999). It is worth noting, however, that several studies have indicated that the effects of clumping and woody area may be compensatory, potentially enabling PAI_e to be used as a proxy of LAI without correction (Fang, 2021; Fang et al., 2019; Schlerf et al., 2005). For deciduous species, WAI can be determined as the PAI measured during leaf-off conditions and subtracted from leaf-on PAI. However, this requires additional sampling during the winter, and is infeasible for evergreen species (Bréda, 2003; Dufrêne and Bréda, 1995; Gower et al., 1999; Yan et al., 2019; Zou et al., 2009).

It is has long been known that leaves reflect and transmit strongly in the near-infrared region of the electromagnetic spectrum (as photons undergo internal scattering at the interface between interstitial air space and the walls of the spongy mesophyll cells), whilst reflectance and transmittance at visible wavelengths is comparatively lower (due to absorption by pigments such as chlorophyll) (Curran, 1989; Gates et al., 1965; Gausman, 1977; Knipling, 1970). Despite this, and with the exception of more costly terrestrial laser scanning (TLS) approaches (Béland et al., 2014; Calders et al., 2018b; Danson et al., 2007, 2014; Douglas et al., 2015; Li et al., 2018), almost all indirect optical in situ LAI measurement techniques rely on visible light, and only a handful of studies have attempted to exploit near-infrared wavelengths to distinguish foliage from other material. One of the first was Baret et al. (1993), who described the early use of near-infrared hemispherical photography with an analogue film camera, enabling foliage to be distinguished from the underlying soil background for downwards-facing images. It is known that tree bark has 'soil-like' reflectance properties (Juola et al., 2022), and that stems and branches have negligible transmittance, making such an approach potentially applicable for distinguishing between foliage and woody material. Nevertheless, having to develop and digitise analogue film meant that the efficiency of the method was necessarily restricted.

The advent of digital cameras opened up new opportunities, since their silicon-based charge coupled device (CCD) and complementary metal oxide semiconductor (CMOS) sensors are inherently sensitive to near-infrared light. Indeed, to avoid near-infrared light contaminating visible imagery, commercially available digital cameras typically contain a blocking filter, which can be removed to restore near-infrared sensitivity (Milton, 2002; Nijland et al., 2014; Petach et al., 2014). Using this principle, Kucharik et al. (1997, 1998) developed an instrument known as the 'multiband vegetation imager (MVI)', which was based on a CCD camera coupled to a visible/near-infrared filter exchange mechanism, whilst Zou et al. (2009) described a similar 'multispectral canopy imager (MCI)' comprised of two co-registered cameras (one acquiring visible and one near-infrared imagery). The primary disadvantage of these systems was their limited field-of-view (10° to 15°), which prevented the efficient measurement of gap fraction for a wide range of zenith and azimuth angles. To derive PAI, WAI and LAI, many manually pointed images had to be acquired and processed (or else ancillary data on canopy leaf angle distribution had to be collected), substantially reducing practicality in the field.

To overcome this drawback, a small number of preliminary studies have since experimented with near-infrared DHP, extending the early work of Baret et al. (1993) to digital rather than analogue film cameras. With a 180° field-of-view, DHP offers full zenithal and azimuthal sampling. Chapman (2007) described the modification of a Nikon Coolpix 950 digital camera, highlighting its potential for distinguishing between foliage and woody material in DHP, whilst Kirby et al. (2018) presented similar results using the Raspberry Pi NoIR coupled to a fisheye lens. Likewise, Osmond (2009) and Konarska et al. (2021) modified Nikon Coolpix 990 and D5100 cameras, respectively, demonstrating their utility for DHP in urban environments by enabling foliage to be distinguished from surrounding buildings and structures. Whilst these preliminary studies have highlighted the promising potential of near-infrared DHP, a comprehensive evaluation against reference WAI values in forest rather than urban environments is lacking. Using data collected at a deciduous broadleaf forest site with both visible and near-infrared digital hemispherical cameras, in this study, we address the following research questions:

1. Can leaf-on near-infrared DHP provide comparable WAI estimates to leaf-off visible DHP?
2. If leaf-on WAI values derived from near-infrared DHP are used to correct estimates of PAI for the effects of woody material, are the results comparable to correction using leaf-off WAI values derived from visible DHP?
3. What magnitude of overestimation in LAI might be expected if no correction for woody material is carried out?
4. To what extent might the effects of clumping and woody area be compensatory?

2. Materials and methods

2.1. Study site

Data collection was carried out at Wytham Woods, Oxfordshire, United Kingdom (51.7734°N, 1.3384°W) (Fig. 1) during leaf-on conditions at the peak of the growing season (20th to 22nd July 2021), and leaf-off conditions during dormancy (23rd March 2022). Leaf-off sampling was undertaken after the peak of the growing season, rather than before, to minimise the effects of cumulative plant growth between the two dates. Note that continuous data acquired by an automated DHP system at Wytham Woods (Brown et al., 2020b) reveal little change in WAI between 2018 and 2022, indicating that any plant growth between July 2021 and March 2022 was minimal (Appendix A). The site is managed by the University of Oxford and affiliated to the UK Environmental Change Network (ECN) and Forest Global Earth Observatory (ForestGEO). It consists of 400 ha of ancient semi-natural woodland dominated by oak (*Quercus robur*), ash (*Fraxinus excelsior*), beech (*Fagus sylvatica),* hazel (*Corylus avellana*), and sycamore (*Acer pseudoplatanus*), with a canopy height of approximately 15 m. Several previous studies have attempted to characterise canopy structure at the site using TLS, DHP, and LAI-2200 measurements (Brown et al., 2020b, 2021a; Calders et al., 2018a, 2018b; Origo et al., 2017), making it a good choice for benchmarking a new measurement approach.

2.2. Data collection

Leaf-on DHP data were collected in ten woodland elementary sampling units (ESUs) (Fig. 1) during the Fiducial Reference Measurement for Vegetation (FRM4VEG) Phase 2 campaign, which took place between 20th and 22nd July 2021 (Table 1). In each ESU, which was approximately 20 m × 20 m in size, images were acquired at 15

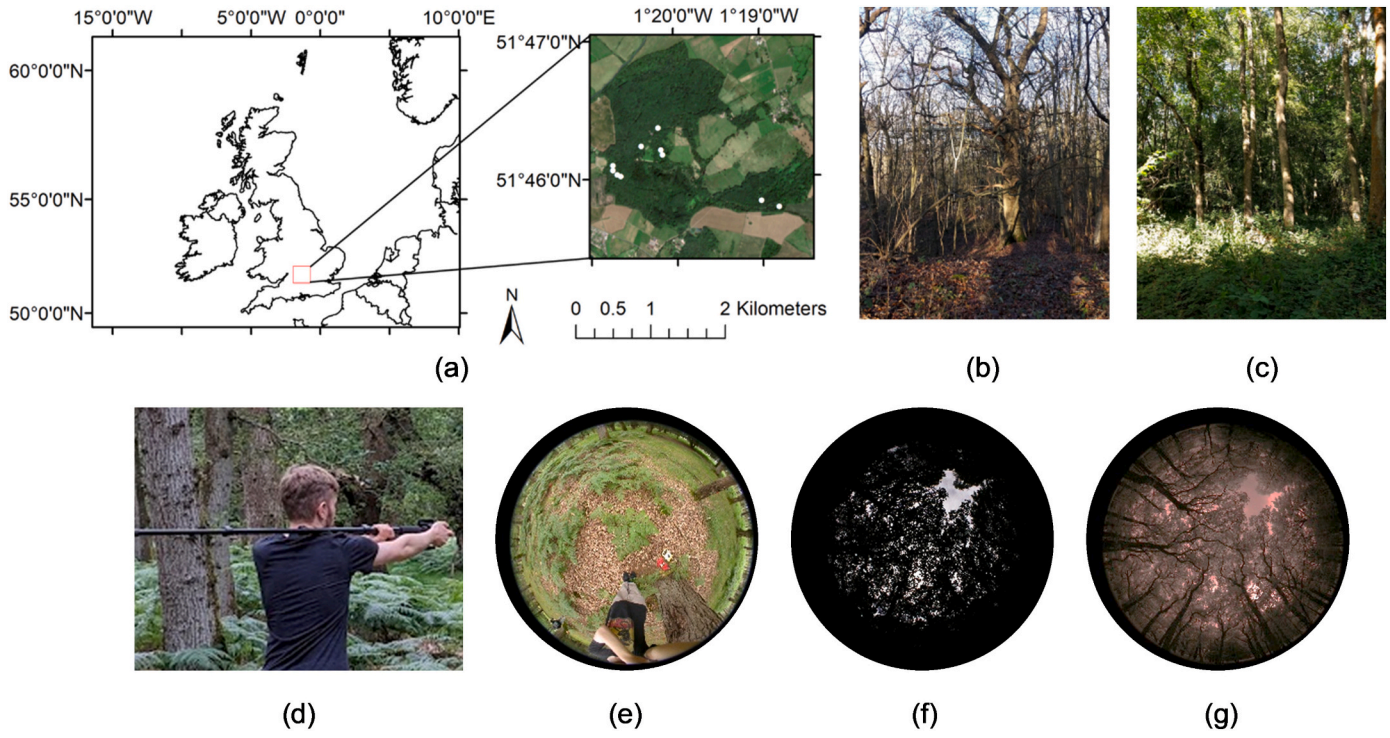

Fig. 1. Location of the study site and ten woodland elementary sampling units (ESUs) at which DHP data were collected (a), in addition to illustrative photographs of the study site during leaf-off (b) and leaf-on (c) conditions (photographs not acquired on DHP measurement dates), image acquisition using the Nikon Coolpix 4500 at shoulder height (d), and example downwards-facing visible (e), upwards-facing visible (f) and upwards-facing near-infrared (g) images. The background image (a) is a Sentinel-2B Multispectral Instrument (MSI) true colour composite acquired on 18th July 2021.

Table 1
Summary of data collection during leaf-on and leaf-off conditions.

Canopy condition	Date	Camera	Fisheye lens	Type of imagery	Image direction	Camera height	Derived variables
Leaf-on	20th to 22nd July 2021	Canon EOS 60D (non-modified)	Sigma 4.5 mm F2.8 EX DC	Visible	Upwards & downwards	1.5 m	PAI_e & PAI
Leaf-on	20th to 22nd July 2021	Nikon Coolpix 4500 (modified)	Nikon FC-E8	Near-infrared	Upwards	1.5 m	WAI_e & WAI
Leaf-off	23rd March 2022	Nikon Coolpix 4500 (non-modified)	Nikon FC-E8	Visible	Upwards	1.5 m	WAI_e & WAI

sampling locations (Fig. 2) (Brown et al., 2021a). Due to the height of the canopy, the DHP footprint was likely to extend beyond the nominal 20 m × 20 m extent of the ESU (Appendix B). As such, care was taken to locate ESUs within larger patches of the same species composition. Images were acquired during daylight hours under overcast conditions suitable for DHP acquisition (Bréda, 2003; Chianucci and Cutini, 2012; Jonckheere et al., 2004). To capture both the overstory and understory, upwards- and downwards-facing visible imagery was acquired with a Canon EOS 60D digital single lens reflex (DSLR) camera equipped with a Sigma 4.5 mm F2.8 EX DC fisheye lens. The EOS 60D was selected due to its large articulating display, enabling the operator to maintain a view of the frame even when the camera was pointing downwards. The camera was held at shoulder height (approximately 1.5 m), rotated manually to face upwards or downwards from this point, and hand-levelled following Origo et al. (2017) with use of a monopod for stabilisation (Fig. 1d).

In addition to visible imagery, upwards-facing near-infrared imagery was acquired with a Nikon Coolpix 4500 camera equipped with an FC-E8 fisheye lens (Table 1). In this case, the camera was modified to restore near-infrared sensitivity, following the approach detailed and illustrated by Chapman (2007) for the Coolpix 950, which is of a very similar design. The first step involved disassembling the side of the camera containing the CCD sensor, before locating and removing the near-infrared blocking filter. Note that the presence of a Bayer filter on the camera's sensor means that when the near-infrared blocking filter is removed, the three bands of the camera become sensitive to near-infrared wavelengths in addition to their original wavelengths (Burggraaff et al., 2019; Nijland et al., 2014). Therefore, a near-infrared bandpass filter was installed, in place of the near-infrared blocking filter, to block visible light from reaching the camera's sensor. We returned to the same ESUs on 23rd March 2022, to collect leaf-off DHP data. In this case, only upwards-facing visible imagery was acquired, using a non-modified Coolpix 4500 and FC-E8 fisheye lens (Table 1).

2.3. Camera spectral characterisation

To better understand the sensitivity of the cameras to different wavelengths, we conducted a laboratory spectral characterisation experiment, in which the modified and non-modified Coolpix 4500 cameras were positioned to view the output of an Oriel 7420 monochromator. The monochromator was equipped with a 1200 lines per mm diffraction grating blazed at 500 nm, and variable entrance and exit slits, which were adjusted to 0.4 mm, yielding a monochromatic light source with a full width at half maximum (FWHM) of approximately 3 nm. The

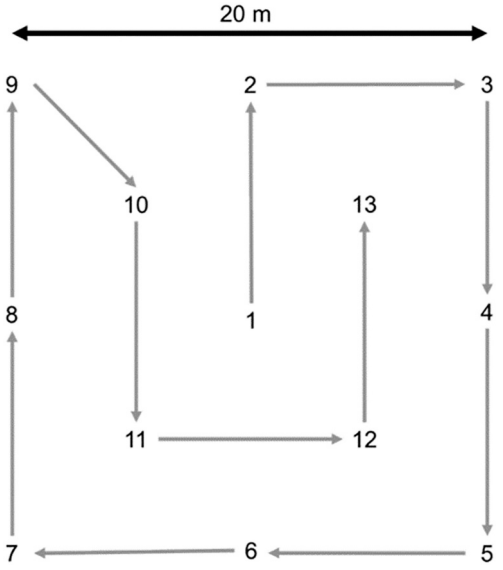

Fig. 2. Within-ESU spatial sampling scheme, in which 13 sampling locations were arranged in a systematic pattern, and a further two sampling locations were randomly located (not shown). Figure adapted from Brown et al. (2021a). (For interpretation of the references to colour in this figure legend, the reader is referred to the web version of this article.)

aperture and shutter speed of the cameras were set to avoid saturation, and were fixed throughout the experiment to ensure a consistent integration period. Images were then acquired whilst the monochromator was adjusted from 400 nm to 900 nm. To account for differences in the intensity of the monochromator's output at different wavelengths, the radiance of the output was measured using a radiometrically calibrated Analytical Spectral Devices (ASD) FieldSpec 3 Visible Near-Infrared (VNIR) spectroradiometer. This enabled the relative intensity of the monochromator's output to be determined at each wavelength interval. Thus, the relative spectral response (RSR) of each band to wavelength λ was calculated as

$$RSR_\lambda = \frac{\overline{DN_\lambda}/k_\lambda}{\max\limits_{400\ nm \le \lambda \le 900\ nm}(\overline{DN_\lambda}/k_\lambda)} \quad (1)$$

where $\overline{DN_\lambda}$ is the mean digital number (DN) value of a region-of-interest covering the centre of the monochromator's exit slit at wavelength λ, and k_λ is the relative intensity of the monochromator's output at that wavelength, which was computed as

$$k_\lambda = \frac{L_\lambda}{\max\limits_{400\ nm \le \lambda \le 900\ nm}(L_\lambda)} \quad (2)$$

where L_λ is the radiance at wavelength λ as measured with the spectroradiometer.

2.4. DHP image processing

Leaf-on visible imagery was used to estimate PAI_e and PAI, whilst leaf-on near-infrared and leaf-off visible imagery was used to estimate effective WAI (WAI_e) and WAI (Table 1). Note that estimating WAI_e and WAI from leaf-on visible imagery is not possible, as visible images correctly exposed for gap fraction estimation demonstrate very little contrast (Fig. 1f) (Woodgate et al., 2016). All DHP images were processed using HemiPy (Brown et al., 2023a), which classifies upwards-facing images using Ridler and Calvard's (1978) clustering algorithm. The option to ignore zero values (which may bias the resulting threshold for circular fisheye images that contain considerable black space) was selected. In the case of the upwards-facing visible imagery, analysis was restricted to the blue band to i) ensure good contrast between the canopy and sky, ii) minimise the effects of chromatic aberration, and iii) minimise the effects of multiple scattering within the canopy (Leblanc et al., 2005; Macfarlane et al., 2014; Zhang et al., 2005). In the case of the upwards-facing near-infrared imagery, analysis was restricted to the red band to enable woody material to be distinguished. It has been shown that the red band typically demonstrates the greatest near-infrared sensitivity (Berra et al., 2015, 2017), and our analysis indicated that the red band provided sensitivity to the widest range of near-infrared wavelengths (Section 3.1). Downwards-facing visible imagery was classified using Meyer and Neto's (2008) colour index-based approach, which separates green vegetation from its underlying background by subtracting the excess green (ExG) from the excess red (ExR) index. Results less than zero are considered the background. The ExG and ExR index were calculated as

$$ExG = 2\,DN_{green} - DN_{red} - DN_{blue} \quad (3)$$

$$ExR = 1.4\,DN_{red} - DN_{green} \quad (4)$$

where DN_{red}, DN_{green}, and DN_{blue} are digital number values in the red, green, and blue bands of the image, respectively.

Once classified, images were divided into six zenith rings, each corresponding to a zenith range of 10°, and each containing 36 azimuth cells. This enabled gap fraction to be determined for a discrete range of zenith and azimuth angles as the number of background pixels within each cell divided by total number of pixels within the cell. To avoid mixed pixels, analysis was restricted to zenith angles of $< 60°$ (Jonckheere et al., 2004; Weiss and Baret, 2017). PAI_e and WAI_e were computed according to Miller (1967) as

$$PAI_e \text{ or } WAI_e = 2\sum_{i=1}^{6} -ln[\overline{P(\theta_i)}]cos(\theta_i)w_i \quad (5)$$

where $\overline{P(\theta_i)}$ is the mean gap fraction in zenith ring i, with central zenith angle θ_i, over all azimuth cells and images, and w_i is its weight. Weights were computed to sum to one (accounting for the zenithal restriction) as

$$w_i = \frac{sin(\theta_i)\mathrm{d}\theta_i}{\sum_{i=1}^{6} sin(\theta_i)\mathrm{d}\theta_i} \quad (6)$$

(Leblanc et al., 2005; LI-COR, 2013). To derive PAI and WAI, the effects of directional apparent clumping (Fang et al., 2018) were accounted for using the logarithm averaging approach of Lang and Yueqin (1986), such that

$$PAI \text{ or } WAI = 2\sum_{i=1}^{6} -\overline{ln[P(\theta_i)]}cos(\theta_i)w_i \quad (7)$$

where $\overline{ln[P(\theta_i)]}$ is the mean of the natural logarithm of gap fraction values in zenith ring i over all azimuth cells and images.

2.5. Assessing near-infrared DHP for woody material correction

Processed PAI_e or PAI values derived from upwards-facing (overstory) and downwards-facing (understory) images were combined to provide a total value, such that

$$PAI = PAI_{up} + PAI_{down} \quad (8)$$

where PAI_{up} and PAI_{down} are PAI_e or PAI values derived from upwards- and downwards-facing images, respectively (Brown et al., 2020a, 2021b, 2023b; Fernandes et al., 2023; Morisette et al., 2006). Note that because the downwards-facing images have a smaller footprint than the upwards-facing images (Appendix B), this assumes that despite their reduced footprint, the 15 replicate measurements are sufficient to adequately represent understory heterogeneity within the ESU. Since

the downwards-facing classification is sensitive only to green vegetation (Meyer and Neto, 2008), it was assumed that values derived from downwards-facing images contained no contribution from woody material. Therefore, total LAI_e or LAI was determined as

$$LAI = PAI_{up} - WAI_{up} + PAI_{down} \quad (9)$$

where WAI_{up} represents the WAI_e or WAI value determined from either i) upwards-facing visible imagery during leaf-off conditions, or ii) upwards-facing near-infrared imagery during leaf-on conditions. In the absence of other reference data, the former approach was considered the 'benchmark', enabling the latter approach based on near-infrared imagery to be evaluated.

3. Results and discussion

3.1. Camera spectral sensitivity

The non-modified Coolpix 4500 was characterised by a spectral response typical of an RGB camera, with peak sensitivity of the red, green, and blue bands observed at approximately 460 nm, 540 nm, and 620 nm, respectively (Fig. 3a). Each band was relatively broad, with a FWHM approaching or exceeding 100 nm, and all bands demonstrated some degree of out-of-band sensitivity. The presence of the near-infrared blocking filter was clearly evident, with negligible sensitivity observed above 680 nm (Fig. 3a). In contrast to the non-modified camera, the modified Coolpix 4500 demonstrated no sensitivity to wavelengths below 680 nm, as a result of its near-infrared bandpass filter (Fig. 3b). In this case, the peak sensitivity of the red, green, and blue bands was at approximately 720 nm, 780 nm, and 780 nm, respectively, and a considerably broader response was observed in all bands, with sensitivity appearing to continue beyond 900 nm (Fig. 3b). Whilst we did not investigate the spectral sensitivity of models other than the Coolpix 4500, it is likely that comparable results would be obtained for any similarly modified digital camera featuring a silicon-based CCD or CMOS sensor, given the inherent sensitivity of such sensors to near-infrared light (Milton, 2002; Nijland et al., 2014; Petach et al., 2014).

3.2. Comparison of WAI_e and WAI derived from leaf-off visible and leaf-on near-infrared imagery

If near-infrared DHP is to be used to derive WAI_e and WAI during leaf-on conditions, a key requirement is that it can provide similar values to those obtained from other WAI_e and WAI estimation methods (though is important to note that because foliage is likely to obscure a varying amount of woody material in the leaf-on near-infrared imagery, but not the leaf-off visible imagery, perfect correspondence is not expected). Our results reveal that leaf-on WAI_e values derived from near-infrared imagery were comparable to leaf-off WAI_e values derived from visible imagery (Fig. 4a), yielding an almost identical mean WAI_e of 0.88 and 0.87, respectively (Table 2). However, the leaf-on WAI_e values derived from near-infrared imagery were subject to slightly greater variability (standard deviation = 0.24, range = 0.80) than the leaf-off WAI_e values derived from visible imagery (standard deviation = 0.17, range = 0.54) (Table 2).

Greater (though still small) differences between the two approaches were observed in the case of WAI (Fig. 4b), where on average, the leaf-on near-infrared imagery slightly overestimated WAI (mean = 1.53) when compared to the leaf-off visible imagery (mean = 1.38) (Table 2). This result is somewhat unexpected, as the occlusion of woody material by leaves in the leaf-on near-infrared imagery should theoretically result in a lower WAI (Bréda, 2003; Dufrêne and Bréda, 1995; Gower et al., 1999). One potential explanation is the occurrence of multiple overlapping leaves, which may act to reduce near-infrared transmittance when compared to single non-overlapping leaves, leading to DN values similar to woody material (and subsequent misclassification). On the other hand, the lower WAI in the leaf-off visible imagery could have equally been due to misclassification. As with WAI_e, leaf-on WAI values derived from the near-infrared imagery were more variable (standard deviation = 0.58, range = 1.80) than the leaf-off WAI values derived from visible imagery (standard deviation = 0.46, range = 1.63) (Table 2). The observed variability may reflect random errors associated with imperfect illumination conditions and image classification. Notably, the values derived in this study are in broad agreement with Calders et al. (2018b), who collected leaf-off DHP, TLS, and LAI-2200 measurements at Wytham Woods in 2015 and 2016, reporting mean values of between 1.26 and 1.90 depending on the adopted method.

3.3. Using leaf-on near-infrared WAI_e and WAI to correct PAI_e and PAI for woody material

Having confirmed that near-infrared DHP can be used to derive WAI_e and WAI in leaf-on conditions, a primary application of the approach is the correction of PAI_e and PAI measurements for woody material, enabling LAI_e and LAI to be determined. Our results indicate that LAI_e calculated by subtracting leaf-on WAI_e (derived from near-infrared imagery) from PAI_e provided an unbiased estimate of LAI_e calculated by subtracting leaf-off WAI_e (derived from visible imagery) from PAI_e (bias = −0.01). Agreement between the two approaches was high, with a root mean square difference (RMSD) of 0.33, normalised RMSD (NRMSD) of 11.41%, and correlation (r) of 0.70 (Fig. 5a). Similar results were obtained for LAI calculated by subtracting leaf-on WAI (derived from near-infrared imagery) from PAI, which also provided a nearly unbiased estimate of LAI calculated by subtracting leaf-off WAI (derived from

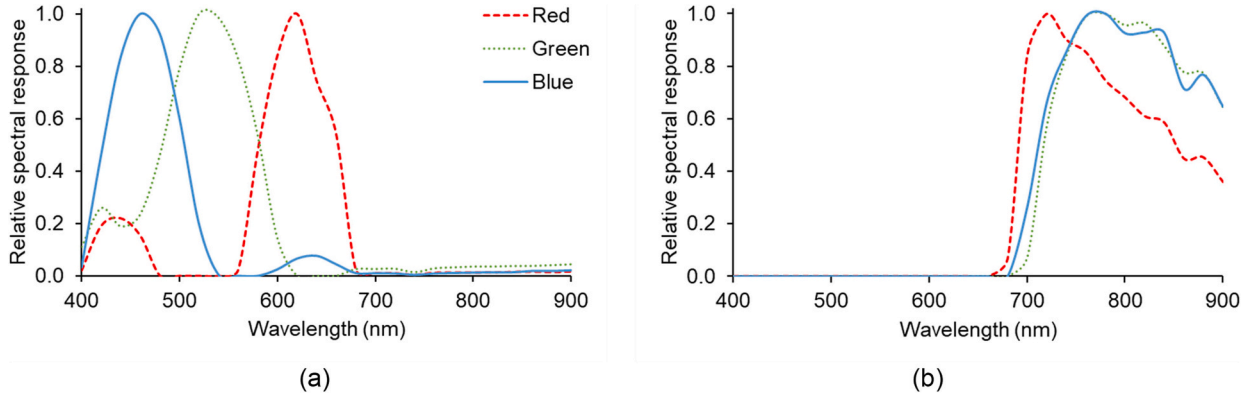

Fig. 3. Relative spectral response of the red, green and blue bands of the non-modified (visible) (a) and modified (near-infrared) (b) Nikon Coolpix 4500 digital cameras to each monochromator input wavelength. (For interpretation of the references to colour in this figure legend, the reader is referred to the web version of this article.)

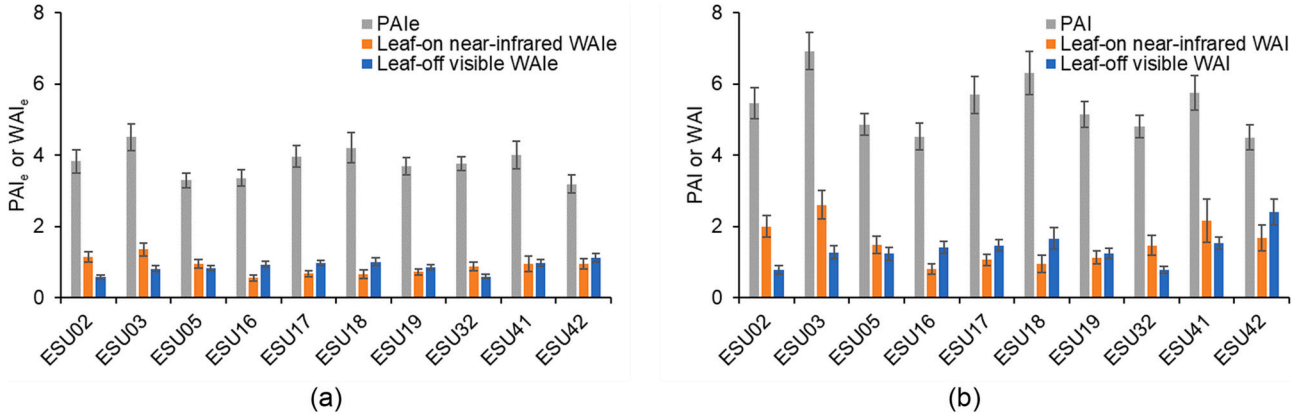

Fig. 4. PAI_e, leaf-on WAI_e (derived from near-infrared imagery), and leaf-off WAI_e (derived from visible imagery) (a), as well as PAI, leaf-on WAI (derived from near-infrared imagery), and leaf-off WAI (derived from visible imagery) (b), in each woodland ESU. Error bars represent expanded uncertainties at the $k = 3$ coverage interval.

Table 2
Summary statistics associated with PAI_e and PAI values derived from leaf-on (visible) imagery WAI_e and WAI values derived from leaf-on (near-infrared) and leaf-off (visible) imagery.

			WAI_e		WAI	
Statistic	PAI_e	PAI	Leaf-on (near-infrared)	Leaf-off (visible)	Leaf-on (near-infrared)	Leaf-off (visible)
Minimum	3.19	4.50	0.55	0.58	0.81	0.77
Maximum	4.51	6.92	1.35	1.12	2.61	2.40
Mean	3.78	5.40	0.88	0.87	1.53	1.38
Standard deviation	0.42	0.79	0.24	0.17	0.58	0.46

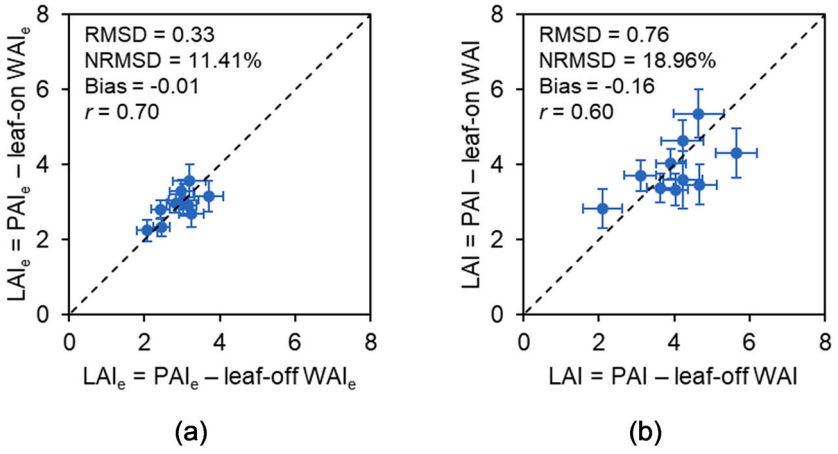

Fig. 5. Relationship between LAI_e (a) and LAI (b) derived by subtracting leaf-off visible and leaf-on near-infrared WAI_e and WAI from PAI_e and PAI. Error bars represent expanded uncertainties at the $k = 3$ coverage interval.

visible imagery) from PAI (bias = −0.16). In this case, a slightly increased RMSD of 0.76 (NRMSD = 18.96%) and decreased correlation ($r = 0.60$) was observed (Fig. 5b).

3.4. Impact of not correcting for woody material

Despite woody material reportedly accounting for up to 35% of total plant area in forests (Gower et al., 1999), in the absence of WAI_e and WAI measurements, many studies have assumed that PAI_e and PAI are equal to LAI_e and LAI (Camacho et al., 2013; De Kauwe et al., 2011; Heiskanen et al., 2012; Verger et al., 2011). The results of this study reveal that, for our study site, estimates of PAI_e overestimated LAI_e by 31% on average, and by 46% in the worst observed case (Table 3), leading to a positive overall bias (0.88) and RMSD of 0.91 (NRMSD =

Table 3
Summary statistics for the degree of underestimation/overestimation in LAI_e and LAI that would be experienced under various assumptions, if no correction for woody material was applied.

	Assumption		
Statistic	$PAI_e = LAI_e$	PAI = LAI	$PAI_e = LAI$
Minimum	20%	18%	−20%
Maximum	46%	61%	52%
Mean	31%	42%	−2%
Standard deviation	8%	18%	20%

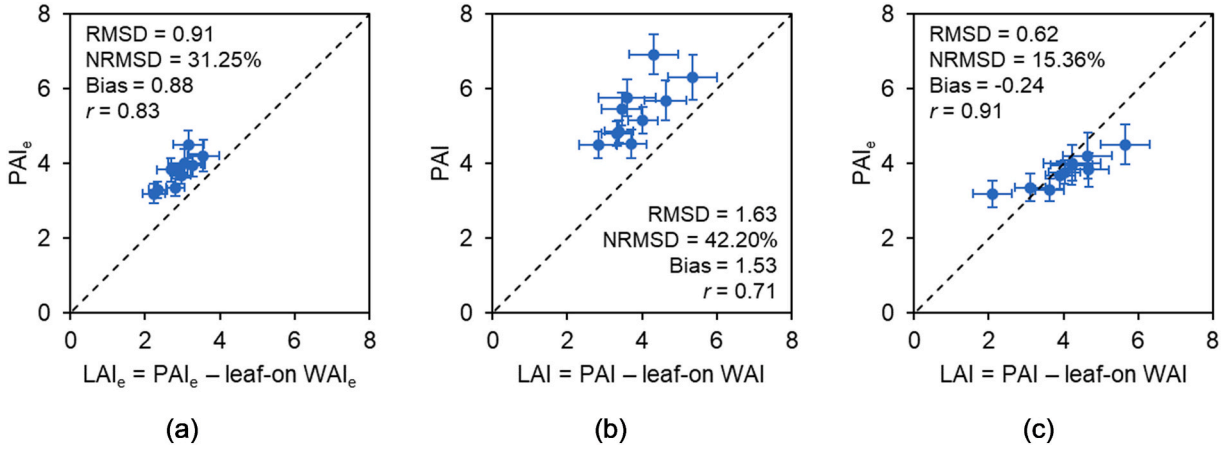

Fig. 6. Relationship between PAI_e and LAI_e (a), PAI and LAI (b), and PAI_e and LAI. Error bars represent expanded uncertainties at the $k = 3$ coverage interval.

31.25%). Despite this overestimation, a strong correlation was observed ($r = 0.83$) (Fig. 6a). Notably, the degree of overestimation was further enlarged when considering estimates of PAI, which overestimated LAI by 42% on average, and 61% in the worst observed case (Table 3), leading to an increased bias (1.53), RMSD (1.63) and NRMSD (42.20%). In this case, a reduced correlation was observed ($r = 0.71$) (Fig. 6b). In agreement with previous studies (Fang, 2021; Fang et al., 2019; Schlerf et al., 2005), we found the effects of clumping and woody area to be partly compensatory, meaning that PAI_e could provide a reasonable approximation of LAI (RMSD = 0.62, NRMSD = 15.36%, bias = −0.24, $r = 0.91$), with an underestimation of 2% on average (Fig. 6c and Table 3). Nevertheless, at the very lowest LAI values, overestimation of 52% was observed, whilst conversely, underestimation of 20% occurred at the highest LAI values (Table 3).

4. Conclusions

The results of this study highlight that woody material can account for a substantial proportion of total plant area in forests. We show that near-infrared DHP can successfully estimate WAI_e and WAI during leaf-on conditions, and that this information can be used to correct estimates of PAI_e and PAI, enabling LAI_e and LAI to be derived with good accuracy. Compared to WAI_e and WAI measurement using leaf-off visible DHP, near-infrared DHP offers two crucial advantages. Firstly, data collection can be conducted at the same time as leaf-on PAI_e and PAI measurements, saving time and expense that would otherwise be associated with additional sampling during the winter period. Secondly, whilst not explicitly evaluated in this study, it is likely that the approach could provide a viable indirect WAI_e and WAI measurement option for evergreen broadleaf species, for which leaf-off conditions are not experienced (and thus for which leaf-off visible DHP is infeasible). Having said this, further evaluation is required for these species, as well as for needleleaf canopies characterised by a very different structure. Whilst not possible in this study due to the conservation status of the study site, additional assessment of the approach against direct, destructive measurements of LAI and WAI should also be undertaken. Unlike previous attempts to use near-infrared imagery for WAI_e and WAI estimation (such as the MVI and MCI), near-infrared DHP is considerably more practical, since its full zenithal and azimuthal sampling means it does not necessitate the acquisition of many manually pointed images or the collection of ancillary data on canopy leaf angle distribution.

CRediT authorship contribution statement

Luke A. Brown: Writing – review & editing, Writing – original draft, Visualization, Validation, Supervision, Software, Resources, Project administration, Methodology, Investigation, Funding acquisition, Formal analysis, Data curation, Conceptualization. **Harry Morris:** Writing – review & editing, Supervision, Investigation, Data curation. **Rosalinda Morrone:** Writing – review & editing, Investigation. **Morven Sinclair:** Writing – review & editing, Investigation. **Owen Williams:** Writing – review & editing, Investigation. **Merryn Hunt:** Writing – review & editing, Investigation. **Subhajit Bandopadhyay:** Writing – review & editing, Investigation. **Xuerui Guo:** Writing – review & editing, Investigation. **Haydar Akcay:** Writing – review & editing, Investigation. **Jadunandan Dash:** Writing – review & editing, Supervision, Resources, Project administration, Funding acquisition.

Data availability

Data will be made available on request.

Acknowledgements

The authors extend their gratitude to Nigel Fisher and the University of Oxford for facilitating access to Wytham Woods, and to Finn James for granting permission to be featured in Fig. 1. The authors are also grateful to the six anonymous reviewers for their constructive comments, which helped to substantially improve the manuscript. This activity was carried out under the Living Planet Fellowship, a programme of and funded by the European Space Agency. The view expressed in this publication can in no way be taken to reflect the official opinion of the European Space Agency. The study has been undertaken using data from "Fiducial Reference Measurements for Vegetation – Phase 2" (FRM4VEG – Phase 2), which was funded by the European Space Agency.

Appendix A

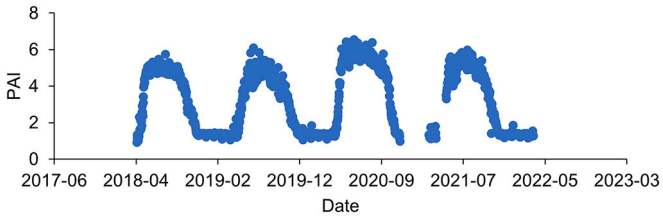

Fig. A1. Time series of PAI derived from an automated DHP system installed at Wytham Woods, demonstrating little change in leaf-off PAI (i.e. WAI) between 2018 and 2022. Further details on the automated DHP system and data processing are provided by Brown et al. (2020b). (For interpretation of the references to colour in this figure legend, the reader is referred to the web version of this article.)

Appendix B

The measurement footprint of a single DHP image can be estimated as

$$2\ h\ tan(\theta) \tag{B1}$$

where h is the distance between the camera and the top (or bottom) of the canopy and θ is the maximum zenith angle analysed (Brown et al., 2020a, 2023b). In our case, for upwards-facing images, $h = 13.5$ m (the camera was held at 1.5 m below a 15 m canopy) (Sections 2.1. and 2.2), and $\theta = 60°$ (Section 2.4), yielding a footprint of approximately 46.8 m. For downwards-facing images, $h = 1.5$ m, yielding a footprint of approximately 5.2 m. By extension, and assuming that the sampling design features measurement locations at the ESU perimeter, as was the case in our study (Fig. 2), the measurement footprint of an ESU can be approximated as

$$2\ h\ tan(\theta) + l \tag{B2}$$

where l is the one-sided length of the ESU (Brown et al., 2020a, 2023b). In our case, $l = 20$ m (Section 2.2), yielding an ESU footprint of approximately 66.8 m for upwards-facing images, and approximately 25.2 m for downwards-facing images.

References

Baret, F., Andrieu, B., Folmer, J.C., Hanocq, J.F., Sarrouy, C., 1993. Gap fraction measurement using hemispherical infrared photographies and its use to evaluate PAR interception efficiency. In: Varlet-Grancher, C., Bonhomme, R., Sinoquet, H. (Eds.), Crop Structure and Light Microclimate: Characterization and Applications. Institut National de la Recherche Agronomique, Paris, France, pp. 359–371.

Béland, M., Baldocchi, D.D., Widlowski, J.-L., Fournier, R.A., Verstraete, M.M., 2014. On seeing the wood from the leaves and the role of voxel size in determining leaf area distribution of forests with terrestrial LiDAR. Agric. For. Meteorol. 184, 82–97. https://doi.org/10.1016/j.agrformet.2013.09.005.

Berra, E., Gibson-Poole, S., MacArthur, A., Gaulton, R., Hamilton, A., 2015. Estimation of the spectral sensitivity functions of un-modified and modified commercial off-the-shelf digital cameras to enable their use as a multispectral imaging system for UAVs. In: Proceedings of the 2015 International Conference on Unmanned Aerial Vehicles in Geomatics. International Society for Photogrammetry and Remote Sensing, Toronto, Canada, pp. 207–214. https://doi.org/10.5194/isprsarchives-XL-1-W4-207-2015.

Berra, E.F., Gaulton, R., Barr, S., 2017. Commercial off-the-shelf digital cameras on unmanned aerial vehicles for multitemporal monitoring of vegetation reflectance and NDVI. IEEE Trans. Geosci. Remote Sens. 55, 4878–4886. https://doi.org/10.1109/TGRS.2017.2655365.

Bréda, N.J.J., 2003. Ground-based measurements of leaf area index: a review of methods, instruments and current controversies. J. Exp. Bot. 54, 2403–2417. https://doi.org/10.1093/jxb/erg263.

Brown, L.A., Meier, C., Morris, H., Pastor-Guzman, J., Bai, G., Lerebourg, C., Gobron, N., Lanconelli, C., Clerici, M., Dash, J., 2020a. Evaluation of global leaf area index and fraction of photosynthetically active radiation products over North America using Copernicus Ground Based Observations for Validation data. Remote Sens. Environ. 247, 111935 https://doi.org/10.1016/j.rse.2020.111935.

Brown, L.A., Ogutu, B.O., Dash, J., 2020b. Tracking forest biophysical properties with automated digital repeat photography: a fisheye perspective using digital hemispherical photography from below the canopy. Agric. For. Meteorol. 287, 107944 https://doi.org/10.1016/j.agrformet.2020.107944.

Brown, L.A., Camacho, F., García-Santos, V., Origo, N., Fuster, B., Morris, H., Pastor-Guzman, J., Sánchez-Zapero, J., Morrone, R., Ryder, J., Nightingale, J., Boccia, V., Dash, J., 2021a. Fiducial reference measurements for vegetation bio-geophysical variables: an end-to-end uncertainty evaluation framework. Remote Sens. 13, 3194. https://doi.org/10.3390/rs13163194.

Brown, L.A., Fernandes, R., Djamai, N., Meier, C., Gobron, N., Morris, H., Canisius, F., Bai, G., Lerebourg, C., Lanconelli, C., Clerici, M., Dash, J., 2021b. Validation of baseline and modified Sentinel-2 Level 2 Prototype Processor leaf area index retrievals over the United States. ISPRS J. Photogramm. Remote Sens. 175, 71–87. https://doi.org/10.1016/j.isprsjprs.2021.02.020.

Brown, L.A., Morris, H., Leblanc, S., Bai, G., Lanconelli, C., Gobron, N., Meier, C., Dash, J., 2023a. HemiPy: a Python module for automated estimation of forest biophysical variables and uncertainties from digital hemispherical photographs. Methods Ecol. Evol. 14, 2329–2340. https://doi.org/10.1111/2041-210X.14199.

Brown, L.A., Morris, H., Meier, C., Knohl, A., Lanconelli, C., Gobron, N., Dash, J., Danson, F.M., 2023b. Stage 1 validation of plant area index from the Global Ecosystem Dynamics Investigation. IEEE Geosci. Remote Sens. Lett. 20, 1–5. https://doi.org/10.1109/LGRS.2023.3319528.

Burggraaff, O., Schmidt, N., Zamorano, J., Pauly, K., Pascual, S., Tapia, C., Spyrakos, E., Snik, F., 2019. Standardized spectral and radiometric calibration of consumer cameras. Opt. Express 27, 19075. https://doi.org/10.1364/OE.27.019075.

Calders, K., Origo, N., Burt, A., Disney, M., Nightingale, J., Raumonen, P., Åkerblom, M., Malhi, Y., Lewis, P., 2018a. Realistic forest stand reconstruction from terrestrial LiDAR for radiative transfer modelling. Remote Sens. 10, 933. https://doi.org/10.3390/rs10060933.

Calders, K., Origo, N., Disney, M., Nightingale, J., Woodgate, W., Armston, J., Lewis, P., 2018b. Variability and bias in active and passive ground-based measurements of effective plant, wood and leaf area index. Agric. For. Meteorol. 252, 231–240. https://doi.org/10.1016/j.agrformet.2018.01.029.

Camacho, F., Cernicharo, J., Lacaze, R., Baret, F., Weiss, M., 2013. GEOV1: LAI, FAPAR essential climate variables and FCOVER global time series capitalizing over existing products. Part 2: validation and intercomparison with reference products. Remote Sens. Environ. 137, 310–329. https://doi.org/10.1016/j.rse.2013.02.030.

Chapman, L., 2007. Potential applications of near infra-red hemispherical imagery in forest environments. Agric. For. Meteorol. 143, 151–156. https://doi.org/10.1016/j.agrformet.2006.12.006.

Chen, J.M., Black, T.A., 1991. Measuring leaf area index of plant canopies with branch architecture. Agric. For. Meteorol. 57, 1–12. https://doi.org/10.1016/0168-1923(91)90074-Z.

Chen, J.M., Cihlar, J., 1995. Plant canopy gap-size analysis theory for improving optical measurements of leaf-area index. Appl. Opt. 34, 6211–6222. https://doi.org/10.1364/AO.34.006211.

Chianucci, F., Cutini, A., 2012. Digital hemispherical photography for estimating forest canopy properties: current controversies and opportunities. iForest Biogeosci. For. 5, 290–295. https://doi.org/10.3832/ifor0775-005.

Curran, P.J., 1989. Remote sensing of foliar chemistry. Remote Sens. Environ. 30, 271–278. https://doi.org/10.1016/0034-4257(89)90069-2.

Danson, F.M., Hetherington, D., Morsdorf, F., Koetz, B., Allgower, B., 2007. Forest canopy gap fraction from terrestrial laser scanning. IEEE Geosci. Remote Sens. Lett. 4, 157–160. https://doi.org/10.1109/LGRS.2006.887064.

Danson, F.M., Gaulton, R., Armitage, R.P., Disney, M., Gunawan, O., Lewis, P., Pearson, G., Ramirez, A.F., 2014. Developing a dual-wavelength full-waveform terrestrial laser scanner to characterize forest canopy structure. Agric. For. Meteorol. 198–199, 7–14. https://doi.org/10.1016/j.agrformet.2014.07.007.

De Kauwe, M.G., Disney, M.I., Quaife, T., Lewis, P., Williams, M., 2011. An assessment of the MODIS collection 5 leaf area index product for a region of mixed coniferous forest. Remote Sens. Environ. 115, 767–780. https://doi.org/10.1016/j.rse.2010.11.004.

Douglas, E.S., Martel, J., Li, Z., Howe, G., Hewawasam, K., Marshall, R.A., Schaaf, C.L., Cook, T.A., Newnham, G.J., Strahler, A., Chakrabarti, S., 2015. Finding leaves in the forest: the dual-wavelength Echidna Lidar. IEEE Geosci. Remote Sens. Lett. 12, 776–780. https://doi.org/10.1109/LGRS.2014.2361812.

Dufrêne, E., Bréda, N., 1995. Estimation of deciduous forest leaf area index using direct and indirect methods. Oecologia 104, 156–162. https://doi.org/10.1007/BF00328580.

Fang, H., 2021. Canopy clumping index (CI): a review of methods, characteristics, and applications. Agric. For. Meteorol. 303, 108374 https://doi.org/10.1016/j.agrformet.2021.108374.

Fang, H., Liu, W., Li, W., Wei, S., 2018. Estimation of the directional and whole apparent clumping index (ACI) from indirect optical measurements. ISPRS J. Photogramm. Remote Sens. 144, 1–13. https://doi.org/10.1016/j.isprsjprs.2018.06.022.

Fang, H., Baret, F., Plummer, S., Schaepman-Strub, G., 2019. An overview of global leaf area index (LAI): methods, products, validation, and applications. Rev. Geophys. 57, 739–799. https://doi.org/10.1029/2018RG000608.

Fernandes, R., Brown, L., Canisius, F., Dash, J., He, L., Hong, G., Huang, L., Le, N.Q., MacDougall, C., Meier, C., Darko, P.O., Shah, H., Spafford, L., Sun, L., 2023. Validation of Simplified Level 2 Prototype Processor Sentinel-2 fraction of canopy cover, fraction of absorbed photosynthetically active radiation and leaf area index products over North American forests. Remote Sens. Environ. 293, 113600 https://doi.org/10.1016/j.rse.2023.113600.

Gates, D.M., Keegan, H.J., Schleter, J.C., Weidner, V.R., 1965. Spectral properties of plants. Appl. Opt. 4, 11–20. https://doi.org/10.1364/AO.4.000011.

Gausman, H.W., 1977. Reflectance of leaf components. Remote Sens. Environ. 6, 1–9. https://doi.org/10.1016/0034-4257(77)90015-3.

GCOS, 2019. Essential Climate Variables [WWW Document]. URL. https://public.wmo.int/en/programmes/global-climate-observing-system/essential-climate-variables (accessed 5.2.19).

Gower, S.T., Kucharik, C.J., Norman, J.M., 1999. Direct and indirect estimation of leaf area index, fAPAR, and net primary production of terrestrial ecosystems. Remote Sens. Environ. 70, 29–51. https://doi.org/10.1016/S0034-4257(99)00056-5.

Heiskanen, J., Rautiainen, M., Stenberg, P., Mõttus, M., Vesanto, V.-H., Korhonen, L., Majasalmi, T., 2012. Seasonal variation in MODIS LAI for a boreal forest area in Finland. Remote Sens. Environ. 126, 104–115. https://doi.org/10.1016/j.rse.2012.08.001.

Jonckheere, I., Fleck, S., Nackaerts, K., Muys, B., Coppin, P., Weiss, M., Baret, F., 2004. Review of methods for in situ leaf area index determination. Agric. For. Meteorol. 121, 19–35. https://doi.org/10.1016/j.agrformet.2003.08.027.

Juola, J., Hovi, A., Rautiainen, M., 2022. A spectral analysis of stem bark for boreal and temperate tree species. Ecol. Evol. 12, 1–14. https://doi.org/10.1002/ece3.8718.

Kirby, J., Chapman, L., Chapman, V., 2018. Assessing the Raspberry Pi as a low-cost alternative for acquisition of near infrared hemispherical digital imagery. Agric. For. Meteorol. 259, 232–239. https://doi.org/10.1016/j.agrformet.2018.05.004.

Knipling, E.B., 1970. Physical and physiological basis for the reflectance of visible and near-infrared radiation from vegetation. Remote Sens. Environ. 1, 155–159. https://doi.org/10.1016/S0034-4257(70)80021-9.

Konarska, J., Klingberg, J., Lindberg, F., 2021. Applications of dual-wavelength hemispherical photography in urban climatology and urban forestry. Urban For. Urban Green. 58, 126964 https://doi.org/10.1016/j.ufug.2020.126964.

Kucharik, C.J., Norman, J.M., Murdock, L.M., Gower, S.T., 1997. Characterizing canopy nonrandomness with a multiband vegetation imager (MVI). J. Geophys. Res. Atmos. 102, 29455–29473. https://doi.org/10.1029/97JD01175.

Kucharik, C.J., Norman, J.M., Gower, S.T., 1998. Measurements of branch area and adjusting leaf area index indirect measurements. Agric. For. Meteorol. 91, 69–88. https://doi.org/10.1016/S0168-1923(98)00064-1.

Lang, A.R.G., Yueqin, X., 1986. Estimation of leaf area index from transmission of direct sunlight in discontinuous canopies. Agric. For. Meteorol. 37, 229–243. https://doi.org/10.1016/0168-1923(86)90033-X.

Leblanc, S.G., Chen, J.M., Fernandes, R., Deering, D.W., Conley, A., 2005. Methodology comparison for canopy structure parameters extraction from digital hemispherical photography in boreal forests. Agric. For. Meteorol. 129, 187–207. https://doi.org/10.1016/j.agrformet.2004.09.006.

Li, Z., Strahler, A., Schaaf, C., Jupp, D., Schaefer, M., Olofsson, P., 2018. Seasonal change of leaf and woody area profiles in a midlatitude deciduous forest canopy from classified dual-wavelength terrestrial lidar point clouds. Agric. For. Meteorol. 262, 279–297. https://doi.org/10.1016/j.agrformet.2018.07.014.

LI-COR, 2013. LAI-2200C Plant Canopy Analyser Instruction Manual. LI-COR, Lincoln, Nebraska, United States.

Macfarlane, C., Ryu, Y., Ogden, G.N., Sonnentag, O., 2014. Digital canopy photography: exposed and in the raw. Agric. For. Meteorol. 197, 244–253. https://doi.org/10.1016/j.agrformet.2014.05.014.

Meyer, G.E., Neto, J.C., 2008. Verification of color vegetation indices for automated crop imaging applications. Comput. Electron. Agric. 63, 282–293. https://doi.org/10.1016/j.compag.2008.03.009.

Miller, J., 1967. A formula for average foliage density. Aust. J. Bot. 15, 141–144. https://doi.org/10.1071/BT9670141.

Milton, E.J., 2002. Low-cost ground-based digital infra-red photography. Int. J. Remote Sens. 23, 1001–1007. https://doi.org/10.1080/01431160110104746.

Morisette, J.T., Baret, F., Privette, J.L., Myneni, R.B., Nickeson, J.E., Garrigues, S., Shabanov, N.V., Weiss, M., Fernandes, R.A., Leblanc, S.G., Kalacska, M., Sanchez-Azofeifa, G.A., Chubey, M., Rivard, B., Stenberg, P., Rautiainen, M., Voipio, P., Manninen, T., Pilant, A.N., Lewis, T.E., Iiames, J.S., Colombo, R., Meroni, M., Busetto, L., Cohen, W.B., Turner, D.P., Warner, E.D., Petersen, G.W., Seufert, G., Cook, R., 2006. Validation of global moderate-resolution LAI products: a framework proposed within the CEOS Land Product Validation subgroup. IEEE Trans. Geosci. Remote Sens. 44, 1804–1817. https://doi.org/10.1109/TGRS.2006.872529.

Nijland, W., de Jong, R., de Jong, S.M., Wulder, M.A., Bater, C.W., Coops, N.C., 2014. Monitoring plant condition and phenology using infrared sensitive consumer grade digital cameras. Agric. For. Meteorol. 184, 98–106. https://doi.org/10.1016/j.agrformet.2013.09.007.

Origo, N., Calders, K., Nightingale, J., Disney, M., 2017. Influence of levelling technique on the retrieval of canopy structural parameters from digital hemispherical photography. Agric. For. Meteorol. 237–238, 143–149. https://doi.org/10.1016/j.agrformet.2017.02.004.

Osmond, P., 2009. Application of near-infrared hemispherical photography to estimate leaf area index of urban vegetation. In: Proceedings of the Seventh International Conference on Urban Climate. International Association for Urban Climate, Yokohama, Japan.

Petach, A.R., Toomey, M., Aubrecht, D.M., Richardson, A.D., 2014. Monitoring vegetation phenology using an infrared-enabled security camera. Agric. For. Meteorol. 195–196, 143–151. https://doi.org/10.1016/j.agrformet.2014.05.008.

Richardson, A.D., Keenan, T.F., Migliavacca, M., Ryu, Y., Sonnentag, O., Toomey, M., 2013. Climate change, phenology, and phenological control of vegetation feedbacks to the climate system. Agric. For. Meteorol. 169, 156–173. https://doi.org/10.1016/j.agrformet.2012.09.012.

Ridler, T.W., Calvard, S., 1978. Picture thresholding using an iterative selection method. IEEE Trans. Syst. Man Cybern. 8, 630–632. https://doi.org/10.1109/TSMC.1978.4310039.

Schlerf, M., Atzberger, C., Hill, J., 2005. Remote sensing of forest biophysical variables using HyMap imaging spectrometer data. Remote Sens. Environ. 95, 177–194. https://doi.org/10.1016/j.rse.2004.12.016.

Sellers, P.J., Dickinson, R.E., Randall, D.A., Betts, A.K., Hall, F.G., Berry, J.A., Collatz, G.J., Denning, A.S., Mooney, H.A., Nobre, C.A., Sato, N., Field, C.B., Henderson-Sellers, A., 1997. Modeling the exchanges of energy, water, and carbon between continents and the atmosphere. Science 275, 502–509. https://doi.org/10.1126/science.275.5299.502.

Verger, A., Baret, F., Camacho, F., 2011. Optimal modalities for radiative transfer-neural network estimation of canopy biophysical characteristics: evaluation over an agricultural area with CHRIS/PROBA observations. Remote Sens. Environ. 115, 415–426. https://doi.org/10.1016/j.rse.2010.09.012.

Weiss, M., Baret, F., 2017. CAN-EYE V6.4.91 User Manual. Institut National de la Recherche Agronomique, Avignon, France.

Welles, J.M., Norman, J.M., 1991. Instrument for indirect measurement of canopy architecture. Agron. J. 83, 818–825. https://doi.org/10.2134/agronj1991.00021962008300050009x.

Woodgate, W., Armston, J.D., Disney, M., Jones, S.D., Suarez, L., Hill, M.J., Wilkes, P., Soto-Berelov, M., 2016. Quantifying the impact of woody material on leaf area index estimation from hemispherical photography using 3D canopy simulations. Agric. For. Meteorol. 226–227, 1–12. https://doi.org/10.1016/j.agrformet.2016.05.009.

Yan, G., Hu, R., Luo, J., Weiss, M., Jiang, H., Mu, X., Xie, D., Zhang, W., 2019. Review of indirect optical measurements of leaf area index: recent advances, challenges, and perspectives. Agric. For. Meteorol. 265, 390–411. https://doi.org/10.1016/j.agrformet.2018.11.033.

Zhang, Y., Chen, J.M., Miller, J.R., 2005. Determining digital hemispherical photograph exposure for leaf area index estimation. Agric. For. Meteorol. 133, 166–181. https://doi.org/10.1016/j.agrformet.2005.09.009.

Zou, J., Yan, G., Zhu, L., Zhang, W., 2009. Woody-to-total area ratio determination with a multispectral canopy imager. Tree Physiol. 29, 1069–1080. https://doi.org/10.1093/treephys/tpp042.